EEET ECOLOGICAL ENGINEERING & ENVIRONMENTAL TECHNOLOGY

Ecological Engineering & Environmental Technology 2024, 25(1), 260–275
https://doi.org/10.12912/27197050/175269
ISSN 2719-7050, License CC-BY 4.0

Received: 2023.11.11
Accepted: 2023.11.29
Published: 2023.12.14

Links between Land Use Change, Land Surface Temperature and Partridge Distribution – An Analysis of Environmental Factors

Kamal El Fallah[1*], Hicham Ouhakki[2], Atman Adiba[3], Khadija El Kharrim[1], Driss Belghyti[1]

[1] Laboratory of Natural Resources and Sustainable Development, Department of Biology, Faculty of Science, University Ibn Toufail, BP 133-14000, Kenitra, Morocco

[2] Laboratory of Organic Chemistry, Catalysis and Environment, Department of Chemistry, Faculty of Science, University Ibn Toufail, BP 133-14000, Kenitra, Morocco

[3] Regional Agricultural Research Center of Meknes, National Institute of Agricultural Research, Avenue Ennasr, P.O. Box 415, Rabat 10090, Morocco

* Corresponding author's e-mail: kamal-meknassi@outlook.com

ABSTRACT

The purpose of this research was to investigate the intricate connections among land use change, land surface temperature, and the distribution of partridges (*Alectoris barbara*), employing a comprehensive analysis of various environmental factors. Indeed, a variety of geospatial techniques have been used to analyze the spatio-temporal trends in temperature as a function of different classes of vegetation cover, and the geographic distribution of ecological niches for this species in Meknes province was modeled using Maxent 3.2 (Maximum Entropy) software. The study spanned a 22-year timeframe, from 2000 to 2021, during which alterations in each land use category were identified through the utilization of various sensors, incorporating Landsat 7 ETM+ and Landsat 8 OLI/TIRS in the analysis. The results induced a significant change in the land surface temperature (LST) with a range of 15.85–36.20°C, 12.76–38.24°C and 25.73–47.79°C for the years 2000, 2010 and 2020, respectively. However, this change was negatively correlated with the normalized difference vegetation index (NDVI). This decline in vegetation, in turn, manifests as a significant factor contributing to the diminution of partridge distribution. By empirically establishing these connections, the research not only underscores the impact of temperature-induced vegetation changes on partridge habitat but also enhances comprehension of the intricate ecological dynamics governing species distribution in the context of evolving land use patterns.

Keywords: ecological niche; *Alectoris barbara*; spatio-temporal analysis; land surface temperature; maximum entropy.

INTRODUCTION

Animals live and move in heterogeneous environments [Johnson et al., 1992]. This heterogeneity affects not only resources such as food, shelter, breeding sites and partners, but also the impact of climate change [Rai et al., 2012]. Given this heterogeneity, the distribution of organisms is often non-random, resulting from the habitat selection processes that are almost universal in the animal kingdom. Understanding the habitat selection process and its structuring (spatial and temporal) is therefore essential, reflecting the structuring of potential population-limiting factors [Northrup et al., 2022]. The partridge is an emblematic bird species of agricultural heritage. It is one of the most common bird species found in agricultural environments [Emmerson et al., 2016]. Its importance is both cultural and socio-economic [Chattopadhyay et al., 2021]. Today, it enjoys an unfavorable conservation status due to a marked decline in abundance throughout the area in which it is native, and the origins of this decline in the partridge have been extensively studied [Raherilalao 2001]. Most of the causes identified are linked directly or indirectly to the intensification of agriculture, but these causes have varied over time. Studies on the decline of the partridge identify major causes linked to the intensification of agriculture, the destruction of nesting habitat, the fall in the availability of insects needed to feed juveniles, and changes in bioclimatic variables, specifically temperature [Emmerson et al., 2016; Préau et al., 2018].

The temperature is a crucial geophysical parameter that has a significant impact on ecological processes such as photosynthesis, plant growth, the distribution and frequency of animal as well as plant species, the regulation of water cycles and the presence of nutrients [Rongali et al., 2018; Gavrilović et al., 2019; Zhang et al., 2022]. The use of remote sensing techniques plays a pivotal role in acquiring data and gathering the information about land surface temperature over large geographical areas at regular intervals without the need for direct contact with the objects or phenomena being studied [Barbieri 2018; Tariq et al., 2020; Al-Taisan 2022; Li et al., 2023]. Remote sensing is a fascinating tool for examining the relationship between surface temperature, land cover and normalized difference vegetation index (NDVI) [Deng et al., 2018; Liu et al., 2021; Alademomi et al., 2022]. Several studies have shown that land use and land cover can have a significant impact on land surface temperature, in fact, different forms of land cover can behave differently in terms of absorbing, reflecting or emitting heat, resulting in disparities in surface temperature [Bai et al., 2019; Yibo et al., 2021]. For remote sensing researchers, exploring the relationship between land surface temperature (LST) and NDVI is a highly interesting research question [Chen et al., 2013; Hu et al., 2019; Malik et al., 2019].

Several studies have shown that the relationship between NDVI and LST can be used to detect signs of climate change, environmental degradation, exaggerated weather events, anthropogenic activities such as agricultural practices, and changes in terrestrial ecosystems [Sandholt et al., 2002; Fontanelli et al., 2012; Tariq et al., 2020; Allam et al., 2021; Ullah et al., 2023]. On the other hand, the images obtained from satellites can be used to map LST and NDVI on a large scale, allowing analysis of long-term trends and changes in the land cover and land surface temperature [Li et al., 2019; Parmar et al., 2022]. Several techniques can be used to estimate land surface temperature from remote sensing data. One of these is the brightness temperature (BT) method, which represents the temperature at which a surface would emit thermal energy if it behaved like a perfect black body. To apply this method [Nguyen et al., 2019; Xing et al., 2021; Nasiri et al., 2022], the data from the thermal infrared bands of satellite images is required [Sajib and Wang, 2020].

The conceptualization of the ecological niche and its subsequent modeling constitute the foundational underpinning for the majority of methodologies crafted to prognosticate the spatial distribution of species [Fabri-ruiz 2019; Brier and lia-dwi, 2020]. The species niche modeling is essential for biodiversity conservation, particularly for endemic and rare species. It is particularly important in the context of environmental change [Toffa et al., 2022]. Maxent (maximum entropy) is an ecological niche modeling model widely used to predict the geographic distribution of species as a function of presence data and environmental variables [Urbani et al., 2017]. It has gained popularity in recent years due to its power and ease of use. One of Maxent's key features is its ability to project and generate the probability maps showing how the potential distribution of a species would change under different scenarios of climate change or changes in environmental variables [Chikerema et al., 2013]. This capability makes it a valuable tool for assessing how species' habitats might evolve in the present and future [Tang et al., 2021].

This research focused on the multi-temporal relationship LULC, NDVI and LST in the areas influenced by climate change with so many droughts on the one hand and anthropogenic effects on the other, knowing that this region is characterized by a specific geographical space and a very fragile natural environment [Karnieli et al., 2010; Ogunjobi et al., 2018; Gogoi et al., 2019]. During the study period, the land cover map of study area was obtained by the supervised likelihood classification method, while the LST and NDVI calculations are based on the data collected by the Landsat sensors in addition; this manuscript has a triple objective. Firstly, the aim of the project was to analyze the spatial and temporal distribution patterns of surface temperature in the study area. Secondly, it sought to examine the correlation between surface temperature and its determinants in various land use categories. Thirdly, it aimed to establish a correlation between ground surface temperature and the normalized difference vegetation index, with a view to predicting the impact of this temperature on the current and future geographical distribution of partridge ecological niches. This study represents the first initiative to assess the consistency of the relationship between LST and NDVI on the one hand and to collect the data on the spatio-temporal evolution of these variables in the city of Meknes (Morocco) on the other hand, with the aim of building a database that can be used in current and future modeling of the ecological niches of different species.

MATERIALS AND METHODS

Description of the study area

According to the latest administrative division of 2015, the prefecture of Meknes is part of the Fez-Meknes region; it covers an area of 1786 km^2, occupies a strategic geographical position, is located on the Saïs plateau between two sets of mountains of the Pre Rif and the Western Middle Atlas, and its territory is crossed by the valley of the Oued Boufakrane (Figure 1). According to the most recent data from the 2014 general population and housing census, the legal population of the prefecture in the majority urban area reached 835,695 inhabitants in 2014 with a density of 468 inhabitants per km^2, among whom 82.3% live in urban areas [Ayanlade et al., 2021]. The region is the second-largest regional metropolis and occupies a very strategic position. In addition to this geographical location, the region offers important economic potential; the fertile plains of Saïs, coupled with abundant water resources, promote human habitation and the establishment of extensive communication networks [Mohajane et al., 2018; Ayanlade et al., 2021].

Data

The USGS Earth Explorer website is a platform used to access a variety of geospatial data; it comprises satellite imagery from a variety of sensors, including Landsat 7 (ETM+) and Landsat 8 (OLI/TIRS). For the research area, this was taken between May 2000 and 2021. Each dataset was pre-processed and projected using the universal projection technique (UTM). The characteristics of the satellite data are presented in Table 1 [USGS 2022]. For this study, all bioclimatic and elevation variable layers were obtained from the WorldClim database at the highest spatial resolution (30 arc seconds (~1 km)). All these layers were processed using QGIS 3.26.3. Partridge distribution data for the study area was gathered through a combination of information sourced from the Global biodiversity information facility (GBIF) at https://www.gbif.org and in situ data in the study area. The application of the Maxent model was employed to ascertain the environmental factors shaping the distribution of partridge and to model the current geographic distribution zones of the species.

Methods

To achieve the study objectives, three fundamental measures were implemented. The initial step involved the identification of LULC types within the research area. The second step was to

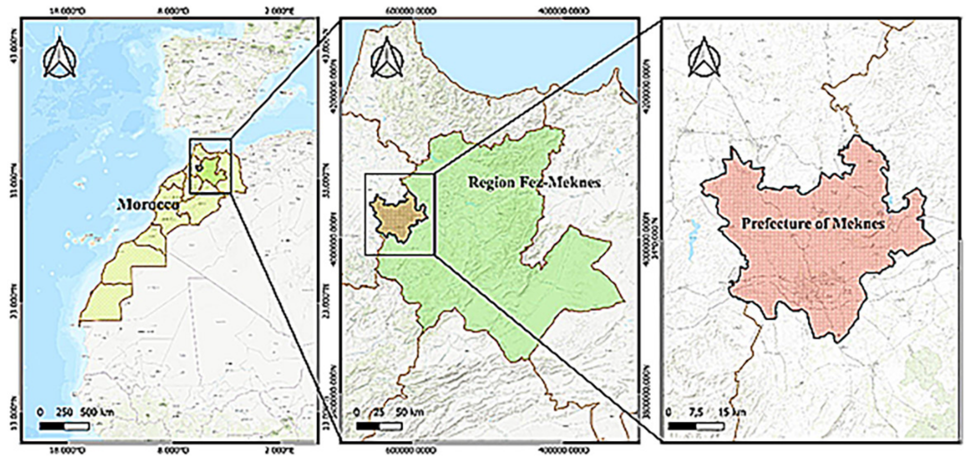

Figure 1. Location of the study area

Table 1. Characteristics of the primary /satellite data used in the present study

Sensor	Date	Resolution	Source
Landsat- 7 ETM+	May 2000	30 m	USGS Earth Explorer
Landsat- 7 ETM+	May 2010	30 m	USGS Earth Explorer
Landsat- 8 OLI/TIRS	May 2021	30 m	USGS Earth Explorer

extract the NDVI for analysis. The third step entailed the extraction of LST from thermal band images of Landsat 7 ETM+ and Landsat 8 OLI/TIRS [Chen et al., 2013]. A statistical analysis of NDVI in conjunction with LST was subsequently employed to assess the changes in LST in correlation with NDVI and, ultimately, to examine its relationship with the different LULC classes [Alademomi et al., 2022]. Figure 2 displays all of the specific methodologies employed in the study.

All acquired images were selected for processing using QGIS 3.26 software. These images were subjected to a supervised classification process by means of the maximum likelihood classification (MLC) method. This process was used for the classification and identification of different types of land use and land cover (LULC) in the study area during the specified period [Viana et al., 2019].

The Landsat 7 ETM+ thermal band 6 and Landsat 8 TIRS bands 10 and 11 were used to determine LST. The four processes listed above must be followed in order to determine the LST using these bands (Table 2) [USGS 2022].

Transforming DN into Spectral Radiance involves applying specific equations provided by the satellite sensor's calibration coefficients. These coefficients vary depending on the sensor and band being used. The equations typically include such factors as gain, offset, and radiometric rescaling parameters [Mujabar 2019]. The pixels of the images are transformed into absolute radiance units according to equation 1 [Ogunjobi et al., 2018].

$$\{L_\lambda = \text{Grescale} * \text{QCAL} + \text{Brescale}\} \quad (1)$$

The equivalent equation was used for the calculation according to the following formula:

$$L_\lambda = ((\text{LMAX}_\lambda - \text{LMIN}_\lambda)/(\text{QCALMAX} - \text{QCALMIN}))\ (\text{QCAL} - \text{QCALMIN}) - \text{LMIN}_\lambda)) \quad (2)$$

where: L_λ – spectral radiance at the sensor aperture (W/(m²·sr·µm)); QCAL – quantized calibrated pixel value (DN); LMIN_λ – Spectral radiance scaled to QCALMIN (W/(m²·sr·µm)), and represented the

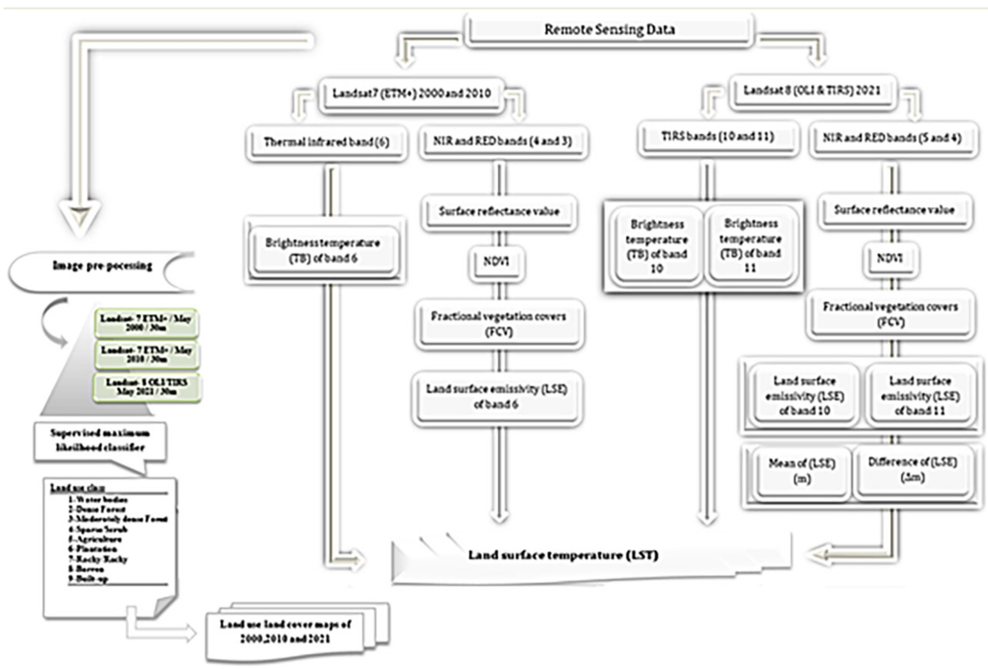

Figure 2. The specific methodologies of the study

Table 2. Description of Landsat7 (ETM+) and Landsat 8 (OLI & TIRS)

No	Landsat 7 (ETM+)			Landsat 8 (OLI & TIRS)		
	Band Name	Resolution (m)	Wavelength (Micrometers)	Band Name	Resolution (m)	Wavelengt (Micromete)
1	Blue	30	0.435–0.451	Ultra-Blue (coastal/ aerosol)	30	0.435–0.451
2	Green	30	0.52–0.60	Blue	30	0.452–0.512
3	Red	30	0.63–0.69	Green	30	0.533–0.590
4	NIR	30	0.77–0.90	Red	30	0.636–0.673
5	SWIR1	30	1.55–1.75	NIR	30	0.851–0.879
6	Thermal	60*(30)	10.40–12.50	SWIR1	30	1.566–1.651
7	SWIR2	30	2.09–2.35	SWIR2	30	2.107–2.294
8	Panchromatic	15	0.52–0.90	Panchromatic	15	0.503–0.676
9				Cirrus	30	1.363–1.384
10				TIRS1	100*(30)	10.60–11.19
11				TIRS2	100*(30)	11.50–12.51

radiance corresponding to the minimum QCAL value used as a reference for calibration; $LMAX_\lambda$ – spectral radiance scaled to QCALMAX (W/(m²·sr·µm)); QCALMIN – minimum quantized and calibrated pixel value (DN); QCALMAX – maximum quantized calibrated pixel value (DN).

The picture pixels are transformed into absolute radiance units [Bodart et al., 2011]. Formula 3 can be expressed as follows:

$$\{L_\lambda = ML * QCAL + AL\} \quad (3)$$

where: L_λ – represents the spectral radiance at a given wavelength (λ), expressed in W/(m²·sr·µm); ML – the slope coefficient, also known as the radiometric calibration slope. It represents the linear relationship between the quantized pixel values (QCAL) and the spectral radiance. The slope coefficient is expressed in W/(m²·sr·µm)/DN; QCAL – this is the quantized pixel value, expressed in digital numbers (DN). It is a discrete measurement that represents the intensity of light captured by the sensor for a specific pixel. AL – this is the offset or intercept of the radiometric calibration. It represents a constant shift that is added to the QCAL value to obtain the corresponding spectral radiance. This is expressed in W/(m²·sr·µm).

To calculate the absolute radiance of a specific pixel, the calibrated pixel value (Q_{CAL}) is multiplied by the multiplicative gain factor (M_L) and then the additive offset (A_L) is added. These specific values (M_L and A_L) depend on the calibration process and the imaging system used. Absolute radiance calculation allows quantitative analysis and interpretation of the image data in terms of radiometric measurements [Mohajane et al., 2018].

Estimation of land surface emissivity

Land surface pixels in satellite pictures are frequently mixed pixels, which means they contain elements of several surface types, including water, plants, and soil. The NDVI threshold approach was used to determine the emissivity of the land surface. This was done using satellite thermal band data. NDVI is used to assess the degree of vegetation cover by analyzing red and near-infrared (NIR) reflectance values to distinguish between the vegetated and non-vegetated areas. The NDVI can be calculated according to equation 4, with the utilization of bands 3 and 4 for the Landsat 7 imagery and bands 4 and 5 for the Landsat 8 imagery [Ayanlade et al., 2021].

$$NDVI = (\lambda NIR - \lambda RED) / (\lambda NIR + \lambda RED) \quad (4)$$

λNIR and λRED represent the reflectance values in the near-infrared (NIR) and red bands, respectively. The NDVI measurements were used to calculate the proportion of vegetation (PV) in accordance with equation 5 [Yue et al., 2007]:

$$Pv = (NDVI - NDVImin/NDVImax - NDVImin)^2 \quad (5)$$

$NDVI_{max}$ represents the NDVI value for densely vegetated land cover, whereas $NDVI_{min}$ corresponds to the NDVI value for non-vegetated land cover. The resulting PV values range from 0 to 1, with 0 corresponding to no vegetation and 1 to complete vegetation cover (Table 3). These values can be used to estimate the emissivity value of the land surface under the following conditions (Eq. (6)).

$$\varepsilon = \begin{cases} \varepsilon_s \; NDVI < 0.2 \\ \varepsilon_v * Pv + \varepsilon_s (1 - Pv) + C_\varepsilon \; 0.2 \le NDVI \le 0.5 \\ \varepsilon_v + C_\varepsilon \; NDVI > 0.5 \end{cases} \quad (6)$$

where: ε_v – the emissivity of the vegetation component. It represents the emissivity of the vegetation cover; ε_s – the emissivity of the non-vegetated (soil) component. It represents the emissivity of the bare ground or non-vegetated surface; Pv – the vegetation cover fraction or vegetation proportion. It represents the proportion of an area that is covered by vegetation. It ranges from 0 to 1, where 0 indicates no vegetation and 1 indicates full vegetation cover; C_e – the emissivity constant or offset, $C\varepsilon = (1- \varepsilon_{s)}\ (1- \varepsilon_v)$.

Emissivity values can vary depending on many factors, such as vegetation type, soil composition, wavelength, temperature, and environmental conditions. Table 3 shows some typical emissivity values for vegetation and bare soil.

Brightness temperature calculation

The brightness temperature (BT) is an approximation of the actual temperature that is measured by a satellite sensor. The Planck equation is commonly used, which relates the spectral radiance (L_λ) of a surface at a given wavelength to the brightness temperature [BT; Qin and Karnieli, 1999]. It is expressed as follows (Eq. (7)).

$$BT = ((K2 \,/\, (\ln((K1/L_\lambda) + 1)) - 273.15 \quad (7)$$

where: BT – is the actual sensor brightness temperature; K1 – calibrating constant 1; K2 – calibrating constant 2; Lλ – the spectral radiance.

To obtain results in Celsius, the radiation temperature is corrected by adding absolute zero (-273.15°C) (Table 4) [Qin and Karnieli, 1999].

Estimation of LST

Equation 8 is one of the common methods for estimating land surface temperature from brightness temperature (BT) [Sajib and Wang, 2020].

$$LST = BT / \left(1 + \lambda \,(BT/\rho) * \ln(\varepsilon_\lambda)\right) \quad (8)$$

where: LST – represents the land surface temperature; BT – represents the brightness temperature in Celsius (°C); λ – the wavelength at which the measurement is made, usually expressed in (μm); ρ – the spectral density of the radiation emitted by the blackbody at temperature BT, expressed in (W/(m²-sr-μm)); ln – the neperian logarithm function; ε_λ – the spectral emissivity, which represents the ability of an object or surface to emit thermal radiation at a given wavelength.

This equation takes into account the influence of surface emissivity and atmospheric effects on the brightness temperature-land temperature relationship.

Table 3. Land surface emissivity of Landsat 7 and 8 thermal bands

Sensor	Bands	Vegetation	Soil
Landsat 7 ETM +	Band 6	0.99	0.973
Landsat 8 Oli/TIRS	Band 10	0.984	0.97

Table 4. K1 and K2 value for Landsat 7 ETM+ and Landsat 8 TIRS bands

Sensor	Landsat 7 ETM +	Landsat 8 TIRS bands	
Band	Band 6	Band 10	Band 11
K1	666.09	1321.08	1201.14
K2	1282.71	777.89	480.89

Statistical analysis

To assess the most significant variables, statistical analysis is crucial. The NDVI and LST were subjected to statistical methods for evaluation by extracting data points from the pixel values of the LST and NDVI images in this study. In total, 1200 sample points were chosen for each study period. The outcomes of the linear regression analysis were then used to create the scatterplots.

RESULTS AND DISCUSSION

LULC mapping

Using the Landsat images from the USGS archive, variation in the different land use and land cover classes was detected throughout the study period (2000, 2010 and 2021). The application of the maximum likelihood supervised classification algorithm on Landsat imagery facilitated the identification and mapping of distinct LULC classes and detection of the changes that have

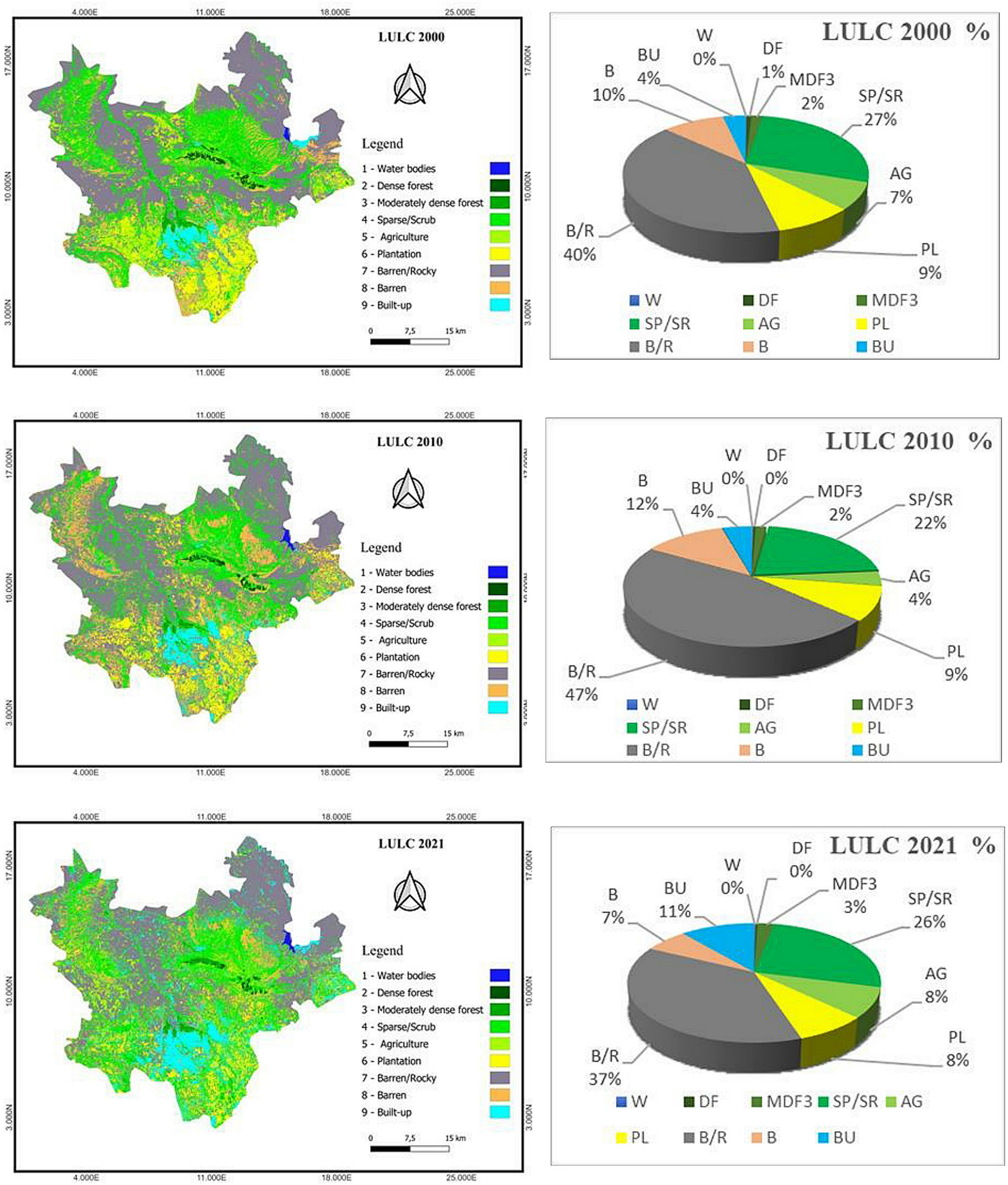

Figure 3. Land use land cover classification map for the year 2000, 2010 and 2021 and percentage of change statistics

occurred in space and time. The results obtained are shown in Figure 3.

According to the statistical analysis carried out, the LULC classes that showed the majority of changes are as follows: there was a reduction in the areas covered by the dense vegetation (-0.46%), sparse/shrubby vegetation (-1.48%), plantations (-1.05%), barren/rocky land (-3.12%), and barren land (-3.15%) classes. In contrast, there was an increase in the areas devoted to agriculture (0.71%), moderately dense forest (0.78%), and built-up areas (7.67%) (Table 5).

The results obtained indicate significant changes in LULC classes over the study period. These changes can be explained by various environmental, socio-economic, and anthropogenic factors, further studies, such as field surveys and socio-economic analyses, were carried out for a more in-depth understanding of the factors responsible for the observed variations.

The decline observed in the Dense Forest, Sparse/scrub, Plantation, Barren/Rocky and Barren classes can be attributed to such processes as climate change, deforestation, urbanization, and the conversion of natural land into barren or artificial areas.

The increase in agricultural, medium-density forest and built-up classes can be explained by such factors as agricultural expansion, population growth and urbanization, while the increase in agricultural land can be due to the conversion of forest land, the introduction of new agricultural practices or the expansion of cash crops. The increase in built-up and urban areas can be due to rapid urbanization, industrial and residential development as well as infrastructure expansion.

Effects of LULC change on NDVI

Figure 4 presents the NDVI images of the Meknes watershed for the years 2001, 2010 and 2021. The obtained NDVI values vary from -0.5 to 0.48 in 2001, -0.65 to 0.55 in 2010 and -0.20 to 0.65 in 2021 (Table 6). Negative to near-zero values generally indicate low vegetation density, while values near 1 indicate high vegetation density and healthier vegetation. These NDVI readings make it possible to compare the vegetation cover in the Meknes catchment over time and to detect possible changes or variations in vegetation density between the different years studied.

Spatio-temporal patterns in LST dynamics

Land surface temperature derivation from the studied region showed substantial spatial and temporal variation. The maps in Figure 5 show that the temperature range from 15.85 to 36.20°C in 2000, 12.76 to 38.24°C in 2010 and 25.73 to 47.79°C in 2021 (Table 7). In turn, the areas with increasing temperatures were indicated in red, the regions with dense plant cover were highlighted in blue as having lower temperatures. The results were in line with the regression analysis, which showed that the surface temperatures of populated areas and arid terrain were higher than those of regions with bodies of water and vegetation.

Exploring the correlation between NDVI dynamics and LST

Scatterplots show an inverse correlation (R^2) between LST and NDVI (Figure 6), which was 0.3682 in 2000, 0.2812 in 2010 and 0.2133 in

Table 5. Land uses Land cover area and change statistics

Land use class	2000 (%)	2010 (%)	2021 (%)	Change in area (%) 2000-2010	Change in area (%) 2010-2021	Change in area (%) 2000-2021
Water bodies	0.11	0.22	0.11	0.11	-0.11	0
Dense Forest	0.79	0.35	0.33	-0.44	-0.02	-0.46
Moderately dense Forest	1.75	1.57	2.53	-0.18	0.96	0.78
Sparse/Scrub	27.41	21.49	25.93	-5.92	4.44	-1.48
Agriculture	7.41	3.92	8.12	-3.49	4.2	0.71
Plantation	8.84	9.17	7.79	0.33	-1.38	-1.05
Barren/Rocky	40.43	46.59	37.31	6.16	-9.28	-3.12
Barren	9.66	12.31	6.51	2.65	-5.8	-3.15
Built-up	3.60	4.38	11.27	0.78	6.89	7.67
Total	100	100	100	0	0	0

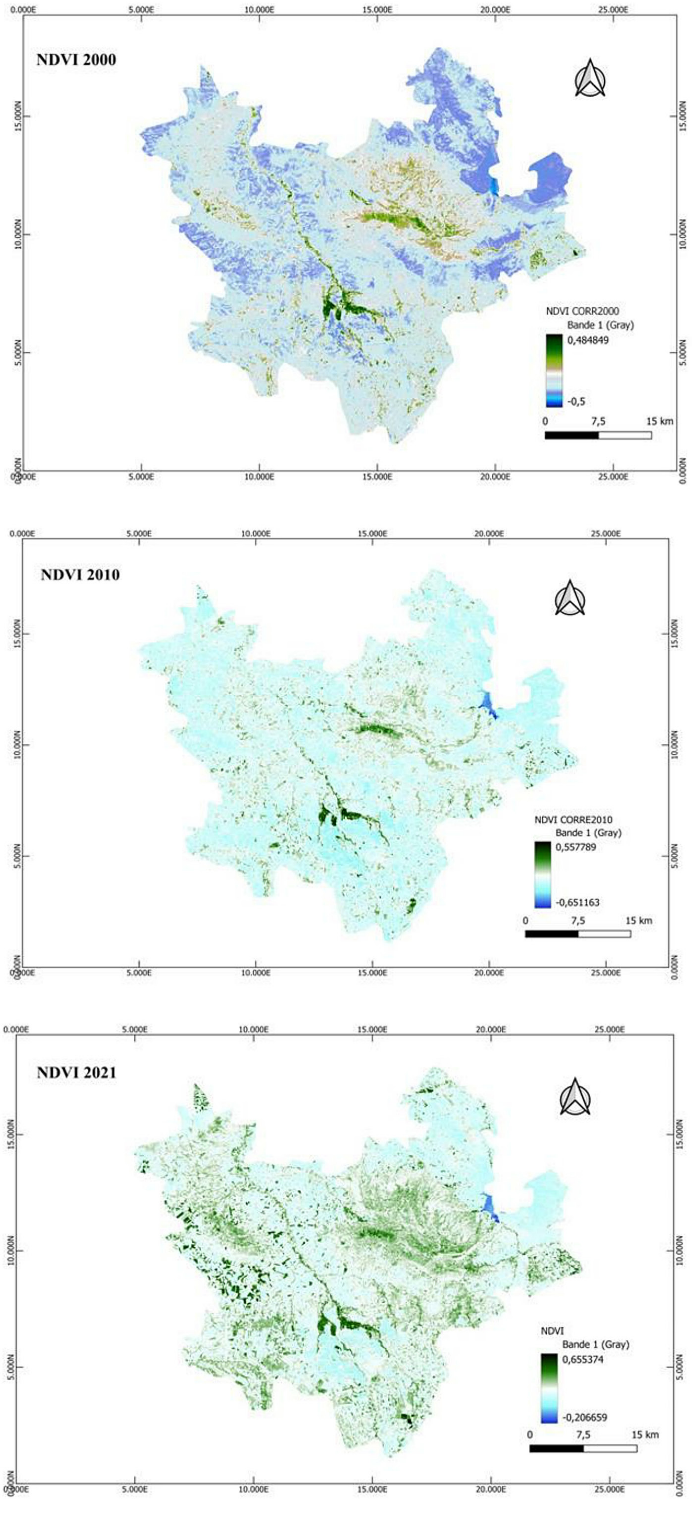

Figure 4. Normalized differential vegetation index maps for the years 2000, 2010 and 2021

Table 6. Statistical summary of NDVI values in Meknes City and its surroundings (2000–2021)

Year	Minimum	Maximum	Mean	Mean NDVI difference		
				2000-2010	2010-2021	2000-2021
May 2000	-0.5	0.48	-0.10			
May 2010	-0.65	0.55	-0.13	-0.03	-0.13	
May 2021	-0.20	0.65	-0.26			

Table 7. Statistical summary of LST (°C) values in Meknes City and its surroundings (2000–2021)

Year	Minimum	Maximum	Mean	Mean LST difference		
				2000-2010	2010-2021	2000-2021
May 2000	15.85	36.20	27.28			
May 2010	12.76	38.24	29.83	2.55	10.10	12.28
May 2021	25.73	47.79	39.93			

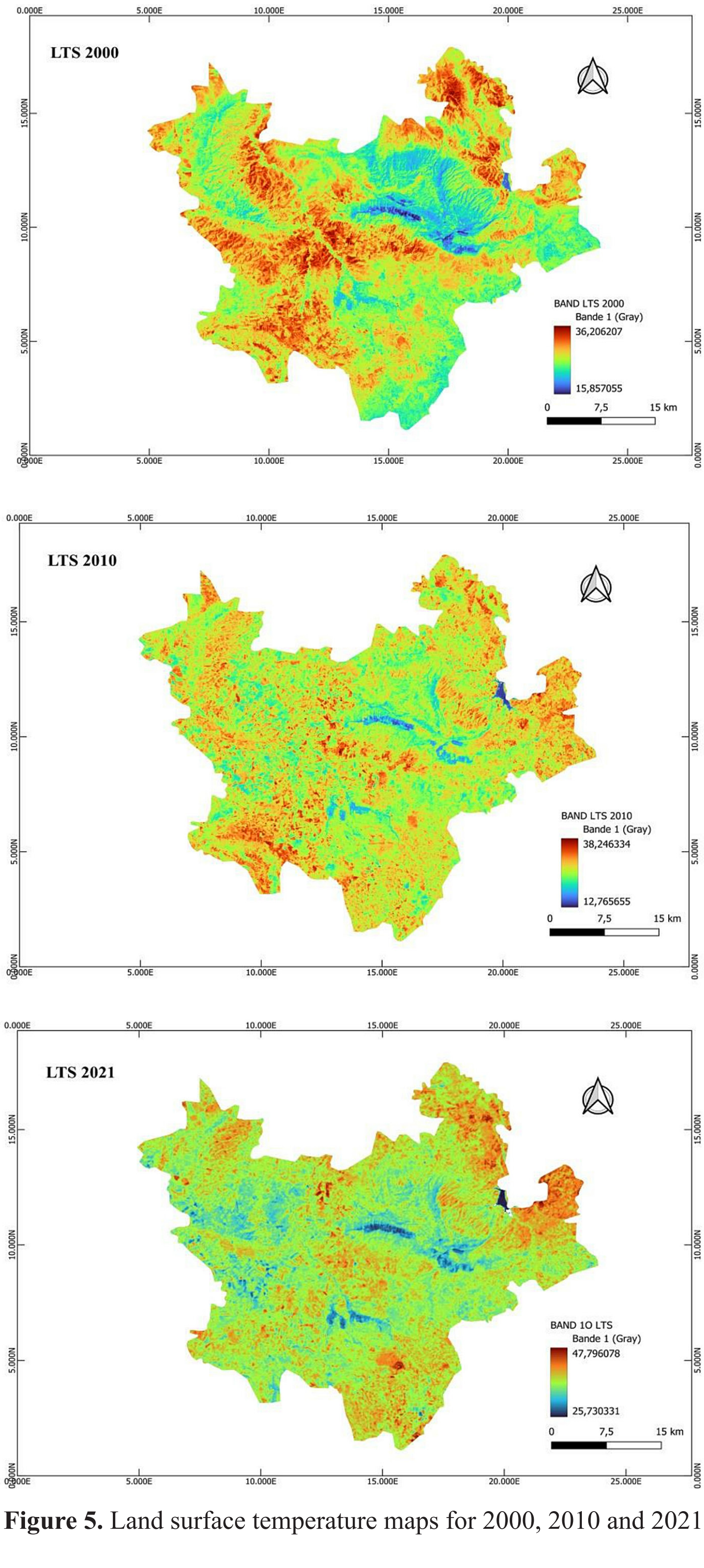

Figure 5. Land surface temperature maps for 2000, 2010 and 2021

Table 8. Linear regression data between NDVI and LTS for the years 2000, 2010 and 2021

Year	Parameter	Value	Error	R	SD	N	P
2000	A	24.59841	0.12547	0.60679	2.5387	1200	<0.001
	B	-16.96928	0.64223				
2010	A	25.57767	0.10829	-0.53027	2.5683	1200	<0.001
	B	-15.3013	0.70682				
2021	A	40.58647	0.19802	-0.4618	2.3409	1200	<0.001
	B	-14.66313	0.81369				

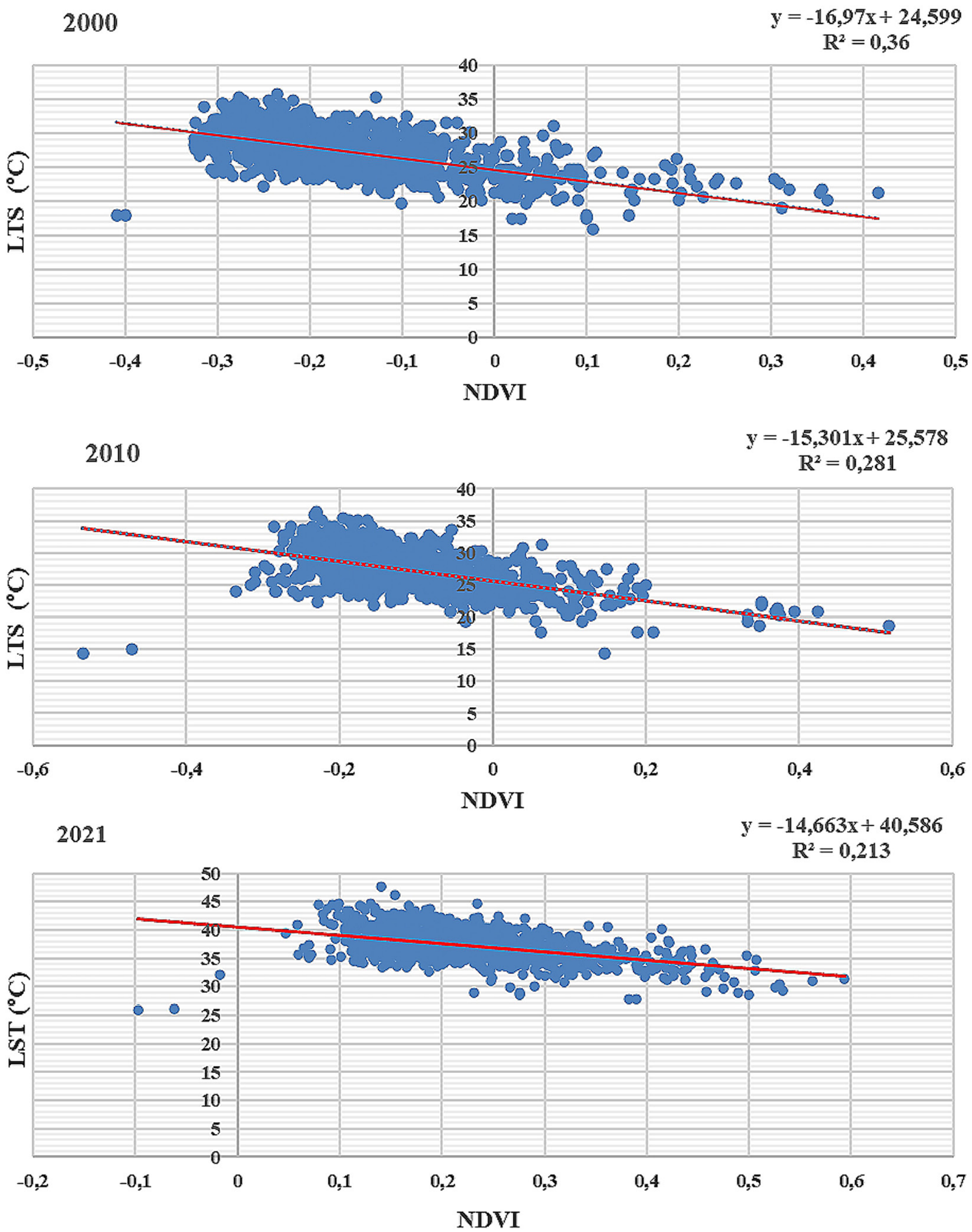

Figure 6. Spatially scattered plots of LST and NDVI of Meknes city and it's surrounding for the years 2000, 2010 and 2021

2021 (Table 8). Similar results have been reported by Naikoo et al. (2020), who revealed that there is an inverse trend between these two variables, where an increase in surface temperature is associated with a decline in NDVI and vice versa. This relationship can be explained by several factors. When the surface temperature increases, it can lead to unfavorable environmental conditions for vegetation. Periods of intense heat can induce heat stress on plants, which can affect their growth and health. As a result, plant density may decrease, reflected in a decrease in NDVI [Allam et al., 2021]. In addition, an increase in surface temperature can lead to an increase in evapotranspiration, the loss of water through evaporation from the soil and plant transpiration. Increased evapotranspiration can reduce water availability for plants, which can also contribute to a decrease in NDVI [Li et al., 2021].

Model evaluations and critical environmental variables

The results obtained by the maximum entropy model for predicting potential habitats for partridges were excellent. The mean AUC value of 0.959 was significantly higher compared to random prediction value (0.5) (Figure 7); this confirms that the predictions were very accurate, suggesting that the potential distribution area results obtained from MaxEnt were reliable and robust [Qin et al., 2017; Jain et al., 2021].

Potential distribution of partridges in the study area

The results obtained are promising for predicting the distribution of partridges in the study area. On the basis of this data, it can be anticipated where these birds are most likely to be found. The geographical distribution map, shown in Figure 8, clearly visualizes these predictions. It should provide a visual overview of the likely distribution of partridges throughout the region.

The escalation in surface temperature has emerged as a pivotal factor exerting discernible impacts on ecological dynamics, particularly manifest in the alteration of normalized difference vegetation indices and subsequent ramifications for the distribution patterns of avian species, exemplified by the partridge in the Moroccan context. In relation to these results, Stralberg et al. (2020) reported that that elevated temperatures induce shifts in vegetation characteristics, thereby influencing the availability of suitable habitats for various species. Similar results were revealed by Kaluskar et al. (2020) who showed the intricate interplay between temperature fluctuations and vegetation dynamics as well as underscored the indispensability of a comprehensive understanding of these ecological relationships between the environmental conditions and the potential distribution of some species under the African climatic conditions. The decline in NDVI, as a proxy for vegetation health and vigor, emerges as a crucial link in this causal chain, delineating a trajectory wherein the temperature-induced

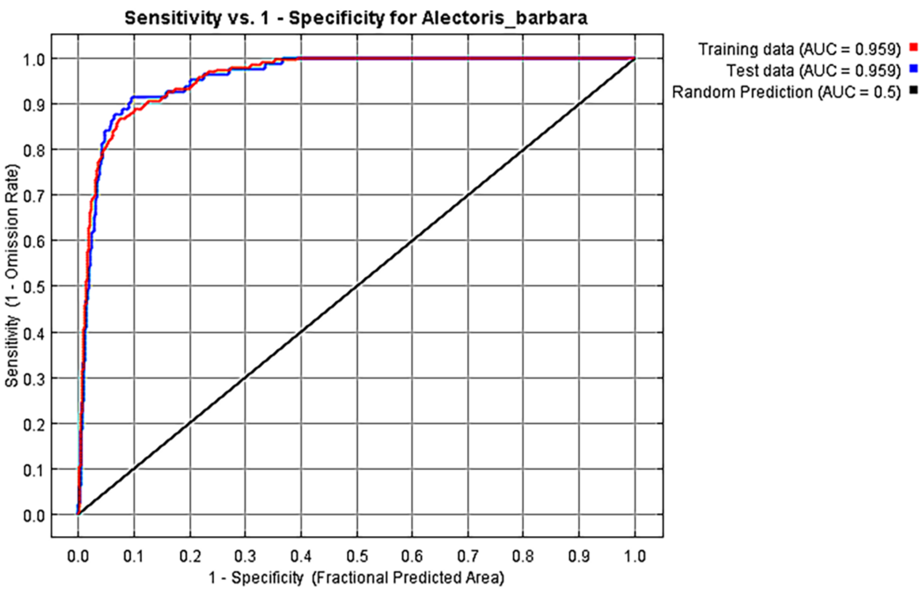

Figure 7. Reliability test of the distribution model created by the MaxEnt t model for Alectoris Barbara

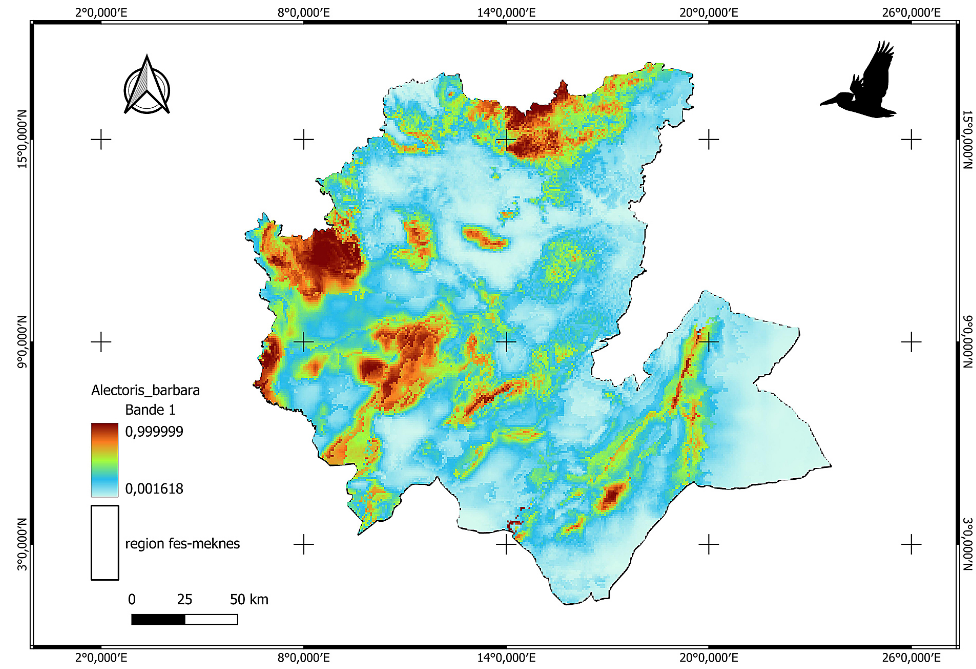

Figure 8. Current distribution model predicted by Maxent in fes-meknes region

alterations reverberate through trophic levels, ultimately impacting the distributional ecology of species, such as the Partridge in the Moroccan landscape. This intricate nexus demands further exploration, with implications for both fundamental ecological theory and applied conservation practices in the face of ongoing climatic perturbations.

CONCLUSIONS

The present study delved into an examination of spatial and temporal dynamics of temperature, land use, and land cover within the Moroccan region, spanning the temporal epochs of 2000, 2010, and 2021. The deduced spatial distribution of land surface temperature, contingent upon the normalized difference vegetation index, was predicated upon multispectral remote sensing data. The obtained results can be used to understand the various environmental changes occurring over the period studied and their impact on terrestrial ecosystems and consequently, on changes in the distribution of partridge ecological niches. Significant changes in land use and land cover classes over time, clearly show that these changes are not uniform, as some classes have regressed, such as Dense Forest, Sparse/Scrub, Plantation, Barren/Rocky and Barren, while others have increased, such as Agriculture, Moderately Dense Forest and Built up. The quantitative analysis between NDVI and LST indicates that there is a negative correlation between the density of the vegetation and the recorded surface temperatures. This finding highlights the beneficial influence of vegetation on the thermal regulation of the environment, where the presence of vegetation helps to reduce local temperatures. These data were used to model the distribution of ecological niches for partridges. This modeling provides an understanding of the environmental conditions that are favorable to the partridge's habitat, as well as the factors that influence its presence or absence in the study region. The present work provides the first map of partridge potential range in the context of current climatic data. This original study for this emblematic species will serve as the basis for any strategic planning for biodiversity conservation and sustainable management of the partridge in Morocco.

Acknowledgements

I am grateful to all those with whom I have enjoyed working during this research.

REFERENCES

1. Alademomi A.S., Okolie C.J., Daramola O.E., Agboola R.O., Salami T.J. 2020. Assessing the relationship of LST, NDVI and EVI with land cover changes in the Lagos Lagoon environment. Quaestiones Geographicae, 39(3), 87–109. https://doi.org/10.2478/quageo-2020-0025

2. Alademomi A.S., Okolie C.J., Daramola O.E., Akinnusi S.A., Adediran E., Olanrewaju H.O., Alabi A.O., Salami T.J., Odumosu J. 2022. Correction to: The interrelationship between LST, NDVI, NDBI, and land cover change in a section of Lagos metropolis, Nigeria. Applied Geomatics, 14(3), 571–572. https://doi.org/10.1007/s12518-022-00446-y
3. Al-Taisan W.A. 2022. A remote sensing approach for displaying the changes in the vegetation cover at Az Zakhnuniyah Island at Arabian Gulf, Saudi Arabia. Scientifica, 1–14. https://doi.org/10.1155/2022/2907921
4. Ayanlade A., Aigbiremolen M.I., Oladosu O.R. 2021. Variations in urban land surface temperature intensity over four cities in different ecological zones. Scientific Reports, 11(1), 1–17. https://doi.org/10.1038/s41598-021-99693-z
5. Bai L., Long D., Yan L. 2019. Estimation of surface soil moisture with downscaled land surface temperatures using a data fusion approach for heterogeneous agricultural land. Water Resources Research. https://doi.org/10.1029/2018WR024162
6. Barbieri T. 2018. A multi-temporal analyses of land surface temperature using Landsat-8 Data and open-source software: the case study of Modena, Italy. https://doi.org/10.3390/su10051678
7. Bodart C., Eva H., Beuchle R., Raši R., Simonetti D., Stibig H.J., Brink A., Lindquist E., Achard F. 2011. Pre-processing of a sample of multi-scene and multi-date Landsat imagery used to monitor forest cover changes over the tropics. ISPRS Journal of Photogrammetry and Remote Sensing, 66(5), 555–563. https://doi.org/10.1016/j.isprsjprs.2011.03.003
8. Brier J., lia-dwi J. 2020. Modélisation de répartition d'espèces aviaires et de feux en forêt boréale du Québec dans un contexte de changement climatique. 21(1), 1–9. http://journal.um-surabaya.ac.id/index.php/JKM/article/view/2203
9. Chattopadhyay B., Forcina G., Garg K.M., Irestedt M., Guerrini M. Barbanera F., & Rheindt F.E. 2021. Novel genome reveals susceptibility of popular gamebird, the red-legged partridge (Alectoris rufa, Phasianidae), to climate change. Genomics, 113(5), 3430–3438. https://doi.org/10.1016/j.ygeno.2021.08.010
10. Chen L., Li M., Huang F., Xu S. 2013. Relationships of LST to NDBI and NDVI in Changsha-Zhuzhou-Xiangtan area based on MODIS data. 6th International Congress on Image and Signal Processing (CISP 2013), Cisp, 840–845. http://en.cnki.com.cn/Article_en/CJFDTOTAL-DLKX200902018.htm
11. Chikerema S.M., Murwira A., Matope G., Pfukenyi D.M. 2013. Spatial modelling of Bacillus anthracis ecological niche in Zimbabwe. Preventive Veterinary Medicine, 111(1–2), 25–30. https://doi.org/10.1016/j.prevetmed.2013.04.006
12. Deng Y., Wang S., Bai X., Tian Y., Wu L., Xiao J., Chen F., Qian Q. 2018. Relationship among land surface temperature and LUCC, NDVI in typical karst area. Scientific Reports, 8(1), 1–12. https://doi.org/10.1038/s41598-017-19088-x
13. DGLA 2015. General monograph of the Fez - Meknes region. https://collectivites-territoriales.gov.ma/fr/node/738
14. Emmerson M., Morales M.B., Oñate J.J., Batáry P., Berendse F., Liira J., Aavik T., Guerrero I., Bommarco R., Eggers S., Pärt T., Tscharntke T., Weisser W., Clement L., Bengtsson J. 2016. How agricultural intensification affects biodiversity and ecosystem services. Advances in Ecological Research, 55, 43–97. https://doi.org/10.1016/bs.aecr.2016.08.005
15. Fabri-ruiz S. 2019. Modèles de distribution et changements environnementaux : Application aux faunes d ' échinides de l ' océan Austral et écorégionalisation To cite this version : HAL Id : tel-02063427 Modèles de distribution et changements environnementaux : Application au.
16. Farah A., Algouti A., Algouti A., Ifkirne M., Rafik A. 2021. Remote sensing for spatio-temporal mapping of land surface temperature and surface energy fluxes in the Bouregreg-Chaouia Region of Morocco. Journal of Environmental and Agricultural Studies, 2(1), 23–35. https://doi.org/10.32996/jeas.2021.2.1.4
17. Fontanelli K., Carla R., Fiorucci F., Santurri L. 2012. Surface soil moisture evaluation by a multitemporal satellite approach. International Geoscience and Remote Sensing Symposium (IGARSS), July, 686–689. https://doi.org/10.1109/IGARSS.2012.6351486
18. Gavrilović M., Pjević M., Borisov M., Marinković G., Petrović V.M. 2019. Analysis of Climate Change in the Area of Vojvodina-Republic of Serbia and Possible Consequences. Journal of Geographical Research, 2(2), 11–19. https://doi.org/10.30564/jgr.v2i2.952
19. Hu X., Ren H., Tansey K., Zheng Y., Ghent D., Liu X., Yan L. 2019. Agricultural drought monitoring using European Space Agency Sentinel 3A land surface temperature and normalized difference vegetation index imageries. Agricultural and Forest Meteorology, 279(August), 107707. https://doi.org/10.1016/j.agrformet.2019.107707
20. Jain D., Areendran G., Raj K., Gupta V.D., Sahana M. 2021. Comparison of ahp and maxent model for assessing habitat suitability of wild dog (cuon alpinus) in pench tiger reserve, madhya pradesh. In Environmental Science and Engineering (Issue October). https://doi.org/10.1007/978-3-030-56542-8_14
21. Johnson A.R., Wiens J.A., Milne B.T., Crist T.O. 1992. Animal movements and population dynamics in heterogeneous landscapes. Landscape Ecology, 7(1), 63–75. https://doi.org/10.1007/BF02573958

22. Kaluskar S., Johnson C.A., Blukacz-Richards E.A., Ouellet F., Kim D.K., Arhonditsis, G. 2020. A stochastic modelling framework to accommodate the inter-annual variability of habitat conditions for Peary caribou (Rangifer tarandus pearyi) populations. Ecological Informatics, 56, 101013.
23. Kumar D., Soni A., Kumar M. 2022. Retrieval of land surface temperature from Landsat-8 thermal infrared sensor data. Journal of Human, Earth, and Future, 3(2), 159–168. https://doi.org/10.28991/HEF-2022-03-02-02
24. Li A., Xia C., Bao C., Yin G. 2019. Using MODIS land surface temperatures for permafrost thermal modeling in beiluhe basin on the Qinghai-Tibet plateau. Sensors (Switzerland), 19(19). https://doi.org/10.3390/s19194200
25. Li B., Liang S., Liu X., Ma H., Chen Y., Liang T., He T. 2021. Estimation of all-sky 1 km land surface temperature over the conterminous United States. In Remote Sensing of Environment (Vol. 266). https://doi.org/10.1016/j.rse.2021.112707
26. Li Z., Wu H., Duan S., Zhao W., Ren H., Liu X., Leng P., Tang R., Ye X., Zhu J., Sun Y., Si M., Liu M., Li J., Zhang X., Shang G., Tang B., Yan G., Zhou C. 2023. Satellite remote sensing of global land surface temperature: definition, methods, products, and applications. Reviews of Geophysics, 61(1). https://doi.org/10.1029/2022rg000777
27. Liu W., Meng Q., Allam M., Zhang L., Hu D., Menenti M. 2021. Driving factors of land surface temperature in urban agglomerations: A case study in the pearl river delta, china. Remote Sensing, 13(15), 1–25. https://doi.org/10.3390/rs13152858
28. Malik M.S., Shukla J.P., Mishra S. 2019. Relationship of LST, NDBI and NDVI using landsat-8 data in Kandaihimmat watershed, Hoshangabad, India. Indian Journal of Geo-Marine Sciences, 48(1), 25–31.
29. Mohajane M., Essahlaoui A., Oudija F., Hafyani M. El Hmaidi A. El Ouali A. El Randazzo G., Teodoro A. C. 2018. Land use/land cover (LULC) using landsat data series (MSS, TM, ETM+ and OLI) in azrou forest, in the central middle atlas of Morocco. Environments - MDPI, 5(12), 1–16. https://doi.org/10.3390/environments5120131
30. Mujabar S.P. 2019. Spatial-temporal variation of land surface temperature of Jubail Industrial City, Saudi Arabia due to seasonal effect by using Thermal Infrared Remote Sensor (TIRS) satellite data. Journal of African Earth Sciences, 155(June 2017), 54–63. https://doi.org/10.1016/j.jafrearsci.2019.03.008
31. Naikoo M. W., Rihan M., Ishtiaque M., Shahfahad. 2020. Analyses of land use land cover (LULC) change and built-up expansion in the suburb of a metropolitan city: Spatio-temporal analysis of Delhi NCR using landsat datasets. Journal of Urban Management, 9(3), 347–359. https://doi.org/10.1016/j.jum.2020.05.004
32. Nasiri V., Deljouei A., Moradi F., Sadeghi S. M.M., Borz S.A. 2022. Land Use and Land Cover Mapping Using Sentinel-2, Landsat-8 Satellite Images, and Google Earth Engine: A Comparison of Two Composition Methods. Remote Sensing, 14(9). https://doi.org/10.3390/rs14091977
33. Nguyen Q.K., Trinh, L.H., Dao, K.H., Dang N.D. 2019. Land Surface Temperature Dynamics in Dry Season 2015-2016 According to Landsat 8 Data in the South-East Region of Vietnam. Geography, Environment, Sustainability, 12(1), 75–87. https://doi.org/10.24057/2071-9388-2018-06
34. Northrup J.M., Vander Wal E., Bonar M., Fieberg J., Laforge M.P., Leclerc M., Prokopenko C.M., Cerber, B.D. 2022. Conceptual and methodological advances in habitat-selection modeling: guidelines for ecology and evolution. Ecological Applications, 32(1), 1–31. https://doi.org/10.1002/eap.2470
35. Ogunjobi K.O., Adamu Y., Akinsanola A.A., Orimoloye I.R. 2018. Spatio-temporal analysis of land use dynamics and its potential indications on land surface temperature in Sokoto Metropolis, Nigeria. Royal Society Open Science, 5(12). https://doi.org/10.1098/rsos.180661
36. Parmar S., Thakur P.K., Chauhan M., Lata R. 2022. Land Use Land Cover Change Detection and Its Impact on Land Surface Temperature of Malana Watershed Kullu, Himachal Pradesh, India. May, 235–263. https://doi.org/10.1007/978-981-16-7731-1_11
37. Préau C., Trochet A., Bertrand R., Isselin-Nondedeu F. 2018. Modeling potential distributions of three european amphibian species comparing enfa and maxent. Herpetological Conservation and Biology, 13(1), 91–104.
38. Qin A., Liu B., Guo Q., Bussmann R.W., Ma F., Jian Z., Xu G., Pei S. 2017. Maxent modeling for predicting impacts of climate change on the potential distribution of Thuja sutchuenensis Franch., an extremely endangered conifer from southwestern China. Global Ecology and Conservation, 10, 139–146. https://doi.org/10.1016/j.gecco.2017.02.004
39. Qin Z., Karnieli A. 1999. Progress in the remote sensing of land surface temperature and ground emissivity using NOAA-AVHRR data. International Journal of Remote Sensing, 20(12), 2367–2393. https://doi.org/10.1080/014311699212074
40. Raherilalao M.J. 2001. Effets de la fragmentation de la forêt sur les oiseaux autour du Parc National de Ranomafana (Madagascar). Revue d'Ecologie (La Terre et La Vie), 56(4), 389–406. https://doi.org/10.3406/revec.2001.2374
41. Rai V., Upadhyay R.K., Thakur N.K. 2012. Complex population dynamics in heterogeneous environments: Effects of random and directed animal movements. International Journal of Nonlinear

Sciences and Numerical Simulation, 13(3–4), 299–309. https://doi.org/10.1515/ijnsns-2012-0115

42. Rongali G., Keshari A.K., Gosain A.K., Khosa R. 2018. Split-Window Algorithm for Retrieval of Land Surface Temperature Using Landsat 8 Thermal Infrared Data. Journal of Geovisualization and Spatial Analysis, 2(2). https://doi.org/10.1007/s41651-018-0021y
43. Sajib M.Q.U., Wang T. 2020. Estimation of land surface temperature in an agricultural region of Bangladesh from landsat 8: Intercomparison of four algorithms. Sensors (Switzerland), 20(6). https://doi.org/10.3390/s20061778
44. Sandholt I., Rasmussen K., Andersen J. 2002. A simple interpretation of the surface temperature/vegetation index space for assessment of surface moisture status. Remote Sensing of Environment, 79(2–3), 213–224. https://doi.org/10.1016/S0034-4257(01)00274-7
45. Stralberg D., Arseneault D., Baltzer J.L., Barber Q.E., Bayne E.M., Boulanger Y., Whitman E. 2020. Climate-change refugia in boreal North America: what, where, and for how long?. Frontiers in Ecology and the Environment, 18(5), 261-270.
46. Tang X., Yuan Y., Li X., Zhang J. 2021. Maximum Entropy Modeling to Predict the Impact of Climate Change on Pine Wilt Disease in China. Frontiers in Plant Science, 12(April). https://doi.org/10.3389/fpls.2021.652500
47. Tariq A., Riaz I., Ahmad Z., Yang B., Amin M., Kausar R., Andleeb S., Farooqi M.A., Rafiq M. 2020. Land surface temperature relation with normalized satellite indices for the estimation of spatio-temporal trends in temperature among various land use land cover classes of an arid Potohar region using Landsat data. Environmental Earth Sciences, 79(1), 1–15. https://doi.org/10.1007/s12665-019-8766-2
48. Toffa Y., Idohou R., Fandohan A.B. 2022. Modélisation de la distribution des espèces en Afrique : état de l'art et perspectives. Physio-Géo, Volume 17, 43–65. https://doi.org/10.4000/physio-geo.13738
49. Ullah W., Ahmad K., Ullah S., Tahir A.A., Javed M.F., Nazir A., Abbasi A.M., Aziz M., Mohamed A. 2023. Analysis of the relationship among land surface temperature (LST), land use land cover (LULC), and normalized difference vegetation index (NDVI) with topographic elements in the lower Himalayan region. Heliyon, 9(2), e13322. https://doi.org/10.1016/j.heliyon.2023.e13322
50. Urbani F., D'Alessandro P., Biondi M. 2017. Using maximum entropy modeling (MaxEnt) to predict future trends in the distribution of high altitude endemic insects in response to climate change. Bulletin of Insectology, 70(2), 189–200.
51. USGS 2020. Landsat 8-9 Operational Land Imager (OLI) - Thermal Infrared Sensor (TIRS) Collection 2 Level 2 (L2) Data Format Control Book (DFCB). Operational Land Imager (OLI) - Thermal Infrared Sensor (TIRS) Data Format Control Book (DFCB. U.S. Geological Survey.
52. Viana C.M., Oliveira S., Oliveira S.C., Rocha J. 2019. Land use/land cover change detection and urban sprawl analysis. In: Spatial Modeling in GIS and R for Earth and Environmental Sciences. Elsevier Inc. https://doi.org/10.1016/b978-0-12-815226-3.00029-6
53. Xing Z., Li Z.L., Duan S.B., Liu X., Zheng X., Leng P., Gao M., Zhang X., Shang G. 2021. Estimation of daily mean land surface temperature at global scale using pairs of daytime and nighttime MODIS instantaneous observations. ISPRS J Photogrammetry and Remote Sensing, 178, 51–67. https://doi.org/10.1016/j.isprsjprs.2021.05.017
54. Yibo Y., Ziyuan C., Xiaodong Y., Simayi Z., Shengtian Y. 2021. The temporal and spatial changes of the ecological environment quality of the urban agglomeration on the northern slope of Tianshan Mountain and the influencing factors. Ecological Indicators, 133(November), 108380. https://doi.org/10.1016/j.ecolind.2021.108380
55. Yu X., Guo X., Wu Z. 2014. Land surface temperature retrieval from landsat 8 TIRS-comparison between radiative transfer equation-based method, split window algorithm and single channel method. Remote Sensing, 6(10), 9829–9852. https://doi.org/10.3390/rs6109829
56. Zhang X., Kasimu A., Liang H., Wei B., Aizizi Y. 2022. Spatial and temporal variation of land surface temperature and its spatially heterogeneous response in the urban agglomeration on the northern slopes of the Tianshan Mountains, Northwest China. International journal Environment Research Public Health, 19(20). https://doi.org/10.3390/ijerph192013067